State of Charge Estimation of Metal Hydride Storage Tank Based on A Switched Observer

Mingrui Chen, Andreu Cecilia, *Member, IEEE*, Ramon Costa-Castelló, *Senior Member, IEEE*, Jing Na, *Member, IEEE* and Carles Batlle

***Abstract*—State of charge is a crucial metric for monitoring and controlling metal hydride storage tanks. However, designing model-based estimators for this system is complex due to the nonlinear, time-varying, and switched dynamics of metal hydride storage tanks, along with operational modes where the system becomes unobservable. This paper proposes a novel nonlinear switched observer for metal hydride storage tanks. Leveraging differential detectability and recent advances in contraction theory for switched systems, we establish sufficient conditions for the observer's convergence, assuming synchronized switching between the observer and the plant. Furthermore, to ensure this synchronization, we propose an unknown system dynamics estimator to identify the current operating mode. The proposed approach is validated through a numerical simulation.**

I. Introduction

Solid-state hydrogen storage is considered a promising technology due to its ability to store hydrogen at high densities under moderate temperature and pressure conditions [1]. Among these technologies, metal hydride (MH) hydrogen storage tanks have attracted considerable attention as key components for solid-state hydrogen storage. This is mainly because MH tanks provide a controlled and gradual release of hydrogen, ensuring a steady supply of gas from the metal hydrides contained within [2], [3].

In MH tanks, the maximum storage capacity is fixed, meaning that exceeding this limit by overfilling with hydrogen can lead to safety risks. As a result, it is essential to continuously monitor the hydrogen content in real-time, which can be quantified by the state of charge (SOC) of the system.

However, estimating SOC in real-time is challenging due to the nonlinear behavior of MH tanks. Suárez et al. [4] approached this problem by calculating the absorbed or desorbed hydrogen mass via an open-loop integration of the flow rate. This method, though useful, requires precise knowledge of the initial hydrogen mass, limiting its real-time application. Moreover, integrating the flow signal directly is prone to sensor noise, and accumulated errors over extended monitoring periods can significantly affect accuracy. Zhu et al. [5] developed a real-time SOC estimation method, utilizing a joint multi-classifier to determine the state of the MH tank. This classifier was then integrated with the SOC model to calculate SOC in real-time. However, this approach requires a large dataset for training the classifier and involves substantial computational costs.

This work aims to estimate the hydrogen and MH densities of a MH tank using a state observer [6]–[8] based on easily measured signals, from which the SOC can then be computed. The main contributions of this paper are as follows:

1) A novel switched nonlinear observer for MH tank systems is introduced.
2) An unknown system dynamics estimator (USDE) for the MH sorption rate is designed [9].
3) The proposed observer is validated through numerical simulation.

The rest of the paper is structured as follows: Section II presents the MH tank model and the SOC estimation problem. Section III explores the observability properties of the MH tank. Section IV introduces the nonlinear observer design. Section V provides numerical validation, and Section VI concludes the paper.

II. MH tank model and Problem Formulation

A. Mathematical Model of MH tanks

The model of the MH tank can be depicted in the following state-space form [10]:

$$\dot{\mathbf{x}} = \mathbf{f}(\mathbf{x}, \mathbf{u}) := \begin{bmatrix} \dfrac{u_2 - f_r(x_2, u_1, \bar{y}(x_1, u_1))}{v_g} \\ \dfrac{f_r(x_2, u_1, \bar{y}(x_1, u_1))}{v_s} \end{bmatrix}, \quad (1)$$

$$\bar{y} = h(\mathbf{x}, \mathbf{u}) := x_1 \frac{u_1 R}{M_{H_2}}. \quad (2)$$

The state vector, $\mathbf{x}$, is defined as $\mathbf{x} = [x_1, x_2]^\top = [\rho_g, \rho_s]^\top$, where:

- ρ_g $[\mathrm{kg/m^3}]$ is the hydrogen gas density.
- ρ_s $[\mathrm{kg/m^3}]$ is the density of the metal hydride.

This work is part of the Project MAFALDA (PID2021-126001OB-C31 funded by MCIN/ AEI /10.13039/50110001 1033 and by "ERDF A way of making Europe") and Project MASHED (TED2021-129927B-I00 funded by MCIN/AEI /10.13039/501100011033 and by the "European Union Next GenerationEU/PRTR"). This work is partially supported by National Natural Science Foundation of China under grant (62273169) and the Chinese Scholarship Council (CSC) under grant (202208530009).

Mingrui Chen and Ramon Costa-Castelló are with the Institut de Robòtica i Informàtica Industrial, CSIC-UPC. C/ Llorens i Artigas 4-6, 08028 Barcelona, Spain. (*Email: chenmingrui2018@gmail.com, ramon.costa@upc.edu*)

Andreu Cecilia and Ramon Costa-Castelló are with the Universitat Politècnica de Catalunya, Avinguda Diagonal, 647, 08028 Barcelona, Spain. (*Email: andreu.cecilia@upc.edu, ramon.costa@upc.edu*)

Jing Na is with the Faculty of Mechanical and Electrical Engineering, Kunming University of Science and Technology, and also with Yunnan Key Laboratory of Intelligent Control and Application, Kunming, 650500, P.R. China. (*Email: najing25@163.com*)

Carles Batlle is with the Departament de Matemàtiques, Institut d'Organització i Control, EPSEVG, UPC, 08800 Vilanova i la Geltru, Spain. (*Email: carles.batlle@upc.edu*)

The model contains two measurable inputs, $\mathbf{u} = [u_1, u_2]^\top = [t_{tank}, f_{in}]^\top$, where:

- t_{tank} [K] is the temperature of the metal hydride tank.
- f_{in} [kg/m^3/s] is the normalized mass flow rate of hydrogen into the tank.

Additionally, the system assumes a measurable output, $\bar{y}$, which is the pressure in the metal hydride tank, p [Pa].

Other parameters included in the model are:

- the universal gas constant, $R = 8.314\,\mathrm{J/mol/K}$.
- the molar mass of hydrogen, $M_{H_2} = 2.016 \times 10^{-3}\,\mathrm{kg/mol}$.

In addition, the normalized hydrogen sorption mass flow rate, f_r, is determined using the following piecewise smooth function:

$$\begin{cases} f_{r,a} = c_a e^{-\frac{E_a}{R\cdot t_{tank}}} \ln\left(\frac{p}{p_{eq,a}}\right)(\rho_{ss}-\rho_s), & p > p_{eq,a}, \\ f_{r,d} = c_d e^{-\frac{E_d}{R\cdot t_{tank}}} \left(\frac{p-p_{eq,d}}{p_{eq,d}}\right)(\rho_s-\rho_{s0}), & p < p_{eq,d}, \\ f_{r,e} = 0, & \text{otherwise.} \end{cases} \tag{3}$$

where:

- c_a [1/s] and c_d [1/s] are the absorption and desorption constants, respectively.
- E_a [J/mol] and E_d [J/mol] are the activation energies for absorption and desorption.
- $p_{eq,a}$ [Pa] and $p_{eq,d}$ [Pa] denote the equilibrium pressures for absorption and desorption, respectively.
- ρ_{ss} [kg/m^3] is the density of the metal hydride when the absorbed hydrogen reaches its saturated density, which can be computed as:

$$\rho_{ss} = \rho_{s0} + \frac{v_{H_2}\cdot\rho_{H_2}}{v_{MH}\cdot(1-\epsilon)} \tag{4}$$

  where v_{H_2} [m^3] is the capacity of hydrogen that can be absorbed by the tank, and ρ_{H_2} [kg/m^3] is the density of hydrogen (1 atm, 0 °C), which is considered a constant. v_{MH} [m^3] and ε are the volume and porosity of the metal hydride.
- ρ_{s0} [kg/m^3] represents the density of the metal alloy without hydrogen.

The equilibrium pressures $p_{eq,a}$ and $p_{eq,d}$, which establish the boundaries for the function switching in (3), are calculated as

$$p_{eq,a} = p_0 \cdot e^{\left(\frac{\Delta S_d}{R} - \frac{\Delta H_d}{R\cdot t_{tank}} + (\varphi+\varphi_0)\tan\left[\pi\left(\frac{\rho_s-\rho_{s0}}{\rho_{ss}-\rho_{s0}}-0.5\right)\right]+\frac{\beta}{2}\right)}, \tag{5}$$

$$p_{eq,d} = p_0 \cdot e^{\left(\frac{\Delta S_d}{R} - \frac{\Delta H_d}{R\cdot t_{tank}} + (\varphi-\varphi_0)\tan\left[\pi\left(\frac{\rho_s-\rho_{s0}}{\rho_{ss}-\rho_{s0}}-0.5\right)\right]-\frac{\beta}{2}\right)}, \tag{6}$$

where:

- p_0 [Pa] is the atmospheric pressure.
- ΔH_d [J/mol] and ΔS_d [J/mol/K] are the enthalpy change and the entropy change for desorption, respectively.
- φ [-] and φ_0 [-] are the plateau flatness coefficients
- β [-] is the plateau hysteresis coefficient.

B. Main objective

The goal of this work is to estimate the SOC of the MH tank which can be computed using the following equation [5]:

$$soc_{tank} \triangleq \frac{m_{H_2}}{m_{total}}, \tag{7}$$

where m_{H_2} [kg] is the current hydrogen mass, and m_{total} [kg] is the tank's maximum hydrogen capacity.

From (1), $v_s\dot{x}_2 + v_g\dot{x}_1 = u_2$ implies that m_{H_2} can be calculated using the initial mass and the integral of the flow rate:

$$\begin{aligned} m_{H_2} &= m_{H_2}(0) + v_{MH}\cdot\int_0^t u_2 dt \\ &= m_{H_2}(0) + v_{MH}\cdot v_s\cdot(x_2 - x_2(0)) \\ &\quad + v_{MH}\cdot v_g\cdot(x_1 - x_1(0)), \end{aligned} \tag{8}$$

where $x_2(0)$ and $x_1(0)$ are the initial densities, and $m_{H_2}(0)$ [kg] is the initial hydrogen mass, given by:

$$m_{H_2}(0) = v_{MH}\cdot v_s\cdot(x_2(0) - \rho_{s0}) + v_{MH}\cdot v_g\cdot x_1(0). \tag{9}$$

Substituting (9) into (8), the SOC can be expressed as:

$$soc_{tank} = \frac{v_{MH}v_g}{m_{total}}x_1 + \frac{v_{MH}v_s}{m_{total}}(x_2 - \rho_{s0}). \tag{10}$$

Since x_1 and x_2 are unknown, the SOC estimation problem becomes an observer design problem. In another word, the goal of this work is to find a dynamic system of the form

$$\dot{\hat{\mathbf{x}}} = F(\hat{\mathbf{x}}, y, \mathbf{u}), \tag{11}$$

with state $\hat{\mathbf{x}} \in \mathbb{R}^2$ and vector field $F : \mathbb{R}^2 \times \mathbb{R} \times \mathbb{R}^2 \to \mathbb{R}^2$, such that for all initial conditions $\mathbf{x}(0) \in \mathbb{R}^2$, $\hat{\mathbf{x}}(0) \in \mathbb{R}^2$, we have

$$\lim_{t\to\infty} \|\mathbf{x}(t) - \hat{\mathbf{x}}(t)\| = 0. \tag{12}$$

Then, the estimation of SOC $\hat{soc}_{tank}$ can be computed as

$$\hat{soc}_{tank} = \frac{v_{MH}v_g}{m_{total}}\hat{x}_1 + \frac{v_{MH}v_s}{m_{total}}(\hat{x}_2 - \rho_{s0}). \tag{13}$$

III. Observability properties of the model

A. Preliminaries

To simplify the presentation, we consider a generic nonlinear system in which the output map is linear:

$$\begin{aligned} \dot{\mathbf{x}} &= \mathbf{f}(\mathbf{x}, \mathbf{u}) \\ \mathbf{y} &= \mathbf{C}\mathbf{x}, \end{aligned} \tag{14}$$

where $\mathbf{x} \in \mathbb{R}^{n_x}$ is the state vector, $\mathbf{y} \in \mathbb{R}^{n_y}$ is the output vector and $\mathbf{u} \in \mathbb{R}^{n_u}$ is the input vector. Moreover, assume that the system (14) is forward invariant in a compact set $\mathbf{X} \subsetneq \mathbb{R}^{n_x}$ uniformly for all $\mathbf{u} \in \mathbf{U} \subsetneq \mathbb{R}^{n_u}$ where $\mathbf{U}$ is also a compact set.

Definition 1 (Differential Detectability, see [11]): The system (14) *is differentially detectable (with respect to an Euclidean metric) uniformly on the input* $\mathbf{u}$ *if there exists a constant positive definite symmetric matrix* $\mathbf{P} \in \mathbb{R}^{n_x\times n_x}$ *and some constants* $\mu, q > 0$ *such that*

$$\mathbf{P}\frac{\partial \mathbf{f}}{\partial \mathbf{x}}(\mathbf{x}, \mathbf{u}) + \frac{\partial \mathbf{f}}{\partial \mathbf{x}}(\mathbf{x}, \mathbf{u})^\top \mathbf{P} - \mu\mathbf{C}^\top\mathbf{C} \preceq -q\mathbf{P} \tag{15}$$

for all $\mathbf{x} \in \mathbf{X}$ *and* $\mathbf{u} \in \mathbf{U}$.

Differential detectability means that for any two system (14) trajectories, denoted by $\mathbf{x}(t)$ and $\mathbf{x}'(t)$, which are indistinguishable based on the output — i.e., $\mathbf{C}\mathbf{x}(t) = \mathbf{C}\mathbf{x}'(t)$ for all $t \geq 0$ under the same input $\mathbf{u} \in \mathbf{U}$ — the trajectories will asymptotically converge to each other. For more information on this property, refer to [11, Section IV].

Additionally, we will introduce the notion of a non-expansive system.

Definition 2 (Non-expansiveness, see [12]): The system (14) *is non-expansive (with respect to an Euclidean metric) uniformly on the input* $\mathbf{u}$ *if there exists a constant positive definite symmetric matrix* $\mathbf{P} \in \mathbb{R}^{n_x \times n_x}$ *such that*

$$\mathbf{P}\frac{\partial \mathbf{f}}{\partial \mathbf{x}}(\mathbf{x}, \mathbf{u}) + \frac{\partial \mathbf{f}}{\partial \mathbf{x}}(\mathbf{x}, \mathbf{u})^\top \mathbf{P} \preceq 0 \tag{16}$$

for all $\mathbf{x} \in \mathbf{X}$ *and* $\mathbf{u} \in \mathbf{U}$.

Non-expansiveness contrasts with the property of contraction, which can be defined as follows:

Definition 3 (Contraction, see [13]): The system (14) *is uniformly contracting if there exists some constants* $a, b > 0$ *such that, for any two trajectories of system* (14)*, denoted as* $\mathbf{x}(t)$*,* $\mathbf{x}'(t)$ *in* $\mathbf{X}$*, and any input* $\mathbf{u} \in \mathbf{U}$ *the following holds for all* $t \geq t_0 \geq 0$

$$\|\mathbf{x}(t) - \mathbf{x}'(t)\| \leq ae^{-bt}\|\mathbf{x}(t_0) - \mathbf{x}'(t_0)\|. \tag{17}$$

B. Observability analysis

Given that the output of the original system contains a bilinear term involving x_1 and u_1, we apply the following transformation to linearize the output (2):

$$y = \bar{y}\frac{M_{H_2}}{u_1 R} = \mathbf{C}\mathbf{x} = \begin{bmatrix}1 & 0\end{bmatrix}\mathbf{x}. \tag{18}$$

Since u_1 is strictly positive, this transformation is always well-defined.

Considering the piecewise function in (3), the entire space $\mathbb{R}^2$ can be partitioned into the following three subsets:

$$\begin{cases} \Omega_1 : \left\{\mathbf{x} \in \mathbb{R}^2, \mathbf{u} \in \mathbb{R}^2 \,|\, p > p_{eq,a}\right\}, \\ \Omega_2 : \left\{\mathbf{x} \in \mathbb{R}^2, \mathbf{u} \in \mathbb{R}^2 \,|\, p_{eq,a} \leq p \leq p_{eq,d}\right\}, \\ \Omega_3 : \left\{\mathbf{x} \in \mathbb{R}^2, \mathbf{u} \in \mathbb{R}^2 \,|\, p < p_{eq,d}\right\}, \end{cases} \tag{19}$$

then the original MH tank model can be rewritten as the following switched system:

$$\begin{aligned} \dot{\mathbf{x}} &= \mathbf{f}_\sigma(\mathbf{x}, \mathbf{u}), \\ y &= \mathbf{C}\mathbf{x} = \begin{bmatrix}1 & 0\end{bmatrix}\mathbf{x}, \end{aligned} \tag{20}$$

where the σ is a switching signal for system dynamics $\mathbf{f}$ with the index set $\mathcal{G} \coloneqq \{1, 2, 3\}$ that is equal to p when $(\mathbf{x}, \mathbf{u}) \in \Omega_p$. The vector field $\mathbf{f}_p$ with $p \in \mathcal{G}$ is defined as

Table I: Parameters of the MH tank model used in the differential detectability analysis

Symbol	Value	Symbol	Value
ϵ	0.6992	v_{MH}	$0.353 \times 10^{-3}\,\mathrm{m}^3$
ρ_{s0}	$6350\,\mathrm{kg/m}^3$	ρ_{H_2}	$0.0897\,\mathrm{kg/m}^3$
R	$8.314\,\mathrm{J/(mol \cdot K)}$	p_0	$101\,325\,\mathrm{Pa}$
M_{H_2}	$2.016 \times 10^{-3}\,\mathrm{kg/mol}$	v_{H_2}	$0.35\,\mathrm{m}^3$
v_{tank}	$0.48 \times 10^{-3}\,\mathrm{m}^3$	ΔS_d	$112.3193\,\mathrm{J/mol/K}$
ΔH_d	$2.6967 \times 10^4\,\mathrm{J/mol}$	φ	0.1770
φ_0	0.0030	β	0.2779
c_a	$843.5713\,1/\mathrm{s}$	c_d	$3109.0\,1/\mathrm{s}$
E_a	$3.2573 \times 10^4\,\mathrm{J/mol}$	E_d	$3.3151 \times 10^4\,\mathrm{J/mol}$

$$\mathbf{f}_1(\mathbf{x}, \mathbf{u}) = \begin{bmatrix} \dfrac{u_2 - f_{r,a}(x_2, u_1, x_1)}{v_g} \\ \dfrac{f_{r,a}(x_2, u_1, x_1)}{v_s} \end{bmatrix},$$
$$\mathbf{f}_2(\mathbf{x}, \mathbf{u}) = \begin{bmatrix} \dfrac{u_2}{v_g} \\ 0 \end{bmatrix}, \tag{21}$$
$$\mathbf{f}_3(\mathbf{x}, \mathbf{u}) = \begin{bmatrix} \dfrac{u_2 - f_{r,d}(x_2, u_1, x_1)}{v_g} \\ \dfrac{f_{r,d}(x_2, u_1, x_1)}{v_s} \end{bmatrix}.$$

We first consider the pressure equilibrium case, i.e. $\mathbf{f} = \mathbf{f}_2$. In this subset, we have that, for all $(\mathbf{x}, \mathbf{u}) \in \Omega_2$,

$$\frac{\partial \mathbf{f}_2}{\partial \mathbf{x}}(\mathbf{x}, \mathbf{u}) = 0. \tag{22}$$

Thus, it is straightforward to confirm that the MH tank model satisfies (16) for any positive and symmetric matrix $\mathbf{P}$, indicating that the system is non-expansive within the region Ω_2. Moreover, the model lacks detectability and observability properties in this region because its vector field is independent of the states.

Now, let us examine the absorption and desorption scenarios, corresponding to regions Ω_1 and Ω_3. For these regions, we verify condition (15) using the convex relaxation method [14]. Specifically, in the analysis, we consider the ranges $u_1 \in [275, 320]$ (K), $u_2 \in [-0.05, 0.13]$ ($\mathrm{kg/m}^3/\mathrm{s}$), $x_1 \in [0.05, 2]$ ($\mathrm{kg/m}^3$), $x_2 \in [6360, 6685]$ ($\mathrm{kg/m}^3$), and the parameters presented in Table I.

In both absorption and desorption conditions, constants are set to $\mu = 40$ and $q = 10$. The matrix $\mathbf{P}$ is chosen as:

$$\mathbf{P} = \begin{bmatrix} 2 & 1 \\ 1 & 1 \end{bmatrix}, \tag{23}$$

which satisfies the inequality:

$$\mathbf{P}\frac{\partial \mathbf{f}_j}{\partial \mathbf{x}}(\mathbf{x}, \mathbf{u}) + \frac{\partial \mathbf{f}_j}{\partial \mathbf{x}}(\mathbf{x}, \mathbf{u})^\top \mathbf{P} - \mu \mathbf{C}^\top \mathbf{C} \leq -q\mathbf{P}, \tag{24}$$

with $j \coloneqq \{1, 3\}$ for the defined sets and parameters.

In summary, from this observability analysis, the MH tank model (1) shows the following certain structural properties:

$$\begin{cases} \Omega_1, \Omega_3: & \text{differential detectable} \\ \Omega_2: & \text{non-expansive} \end{cases} \tag{25}$$

IV. Observer design of the MH tank model

A. Proposal

In this work, we propose the following observer

$$\dot{\hat{\mathbf{x}}} = F_\sigma(\hat{\mathbf{x}}, y, \mathbf{u}) := \mathbf{f}_\sigma(\hat{\mathbf{x}}, \mathbf{u}) + \frac{\mu}{2}\mathbf{P}^{-1}\mathbf{C}^\top(y - \mathbf{C}\hat{\mathbf{x}}), \tag{26}$$

where $\mathbf{f}_\sigma$ is the switched vector field defined in (21), μ and the metric $\mathbf{P}$ are defined in (23).

Assumption 1: The observer (26) and the MH tank (20) have a synchronized switching.

Remark 1: This may be a very strong assumption, considering that part of the state vector is completely unknown. Nonetheless, we offer a strategy for achieving such synchronization in Section IV-B.

Lemma 1: Consider the system described in (20)*, along with the observer defined in* (26)*. Assume that condition* (24) *holds for symmetric positive definite matrix* $\mathbf{P} = \mathbf{P}^\top > 0$ *and positive constants* $\mu > 0$ *and* $q > 0$*. Then, for each mode* $i \in \mathcal{G}$*, the Lyapunov function* $V_i = (\mathbf{x} - \hat{\mathbf{x}})^\top \mathbf{P}(\mathbf{x} - \hat{\mathbf{x}})$ *satisfies the following inequalities for all* $(\mathbf{x}, \mathbf{u}) \in \Omega_i$ *and* $(\hat{\mathbf{x}}, \mathbf{u}) \in \Omega_i$*:*

$$\dot{V}_1 \leq -qV_1, \quad \dot{V}_2 \leq 0, \quad \dot{V}_3 \leq -qV_3. \tag{27}$$

Proof: Let $\tilde{\mathbf{x}} := \mathbf{x} - \hat{\mathbf{x}}$. Given that $\mathbf{f}_i$ is continuously differentiable for all $i \in \mathcal{G}$, the following identity holds for all $i \in \mathcal{G}$:

$$\mathbf{f}_i(\mathbf{x}, \mathbf{u}) - \mathbf{f}_i(\hat{\mathbf{x}}, \mathbf{u}) = \left(\int_0^1 \frac{\partial \mathbf{f}_i}{\partial \mathbf{x}}(\hat{\mathbf{x}} + s\tilde{\mathbf{x}}, \mathbf{u}) ds \right) \tilde{\mathbf{x}} \tag{28}$$

for all $(\mathbf{x}, \mathbf{u}) \in \Omega_i$ and $(\hat{\mathbf{x}}, \mathbf{u}) \in \Omega_i$. Using this identity, we will now prove the first inequality in (27). By differentiating V_1 and applying (28), we get for all $(\mathbf{x}, \mathbf{u}) \in \Omega_1$ and $(\hat{\mathbf{x}}, \mathbf{u}) \in \Omega_1$:

$$\begin{aligned} \dot{V}_1 &= 2\tilde{\mathbf{x}}^\top \mathbf{P}\left(\mathbf{f}_1(\mathbf{x}, \mathbf{u}) - \mathbf{f}_1(\hat{\mathbf{x}}, \mathbf{u})\right) \\ &= 2\tilde{\mathbf{x}}^\top \mathbf{P}\left(\int_0^1 \frac{\partial \mathbf{f}_1}{\partial \mathbf{x}}(\hat{\mathbf{x}} + s\tilde{\mathbf{x}}, \mathbf{u}) ds \right) \tilde{\mathbf{x}} \\ &\leq \tilde{\mathbf{x}}^\top \left[\int_0^1 \left(\mathbf{P}\frac{\partial \mathbf{f}_1}{\partial \mathbf{x}}(\hat{\mathbf{x}} + s\tilde{\mathbf{x}}, \mathbf{u}) + \frac{\partial \mathbf{f}_1}{\partial \mathbf{x}}(\hat{\mathbf{x}} + s\tilde{\mathbf{x}}, \mathbf{u})^\top \mathbf{P} \right) ds \right] \tilde{\mathbf{x}} \\ &\leq -qV_1, \end{aligned}$$

where the last inequality is derived from (24). The other two inequalities can be proved similarly. ∎

Theorem 1: Consider the system (20) *and observer* (26)*. Suppose condition* (24) *holds for some symmetric positive definite matrix* $\mathbf{P} = \mathbf{P}^\top > 0$ *and positive constants* $\mu > 0$ *and* $q > 0$*. Let* $T_p(t_i, t_{i+1})$ *denote the total time that* $\sigma(t) = p$ *during the interval* $[t_i, t_{i+1})$*. Then, for any switching signal* $\sigma : [t_0, \infty) \to \mathcal{G}$ *and corresponding switching instants* $\mathfrak{G} := \{t_1, t_2, \ldots, t_k, \ldots\}$*, if*

$$T_1(t_0, t) + T_3(t_0, t) \geq c(t - t_0), \quad \forall t \geq t_0 \tag{29}$$

holds for some constant $0 < c \leq 1$*, then the switched observer system* (26) *is uniformly contracting according to Definition 3, and the observer error satisfies* (12) *for all* $t \geq t_0 \geq 0$*.*

Proof: This proof is inspired by the developments in [15]. Starting from the switched observer (26), consider the following family of time-varying linear switched systems for all $p \in \mathcal{G}$:

$$\dot{\boldsymbol{\xi}} = \frac{\partial F_p}{\partial \hat{\mathbf{x}}}(\hat{\mathbf{x}}, y, \mathbf{u})\boldsymbol{\xi} = \left(\frac{\partial \mathbf{f}_p}{\partial \mathbf{x}}(\hat{\mathbf{x}}, \mathbf{u}) - \frac{1}{2}\mu\mathbf{P}^{-1}\mathbf{C}^\top\mathbf{C} \right) \boldsymbol{\xi}, \tag{30}$$

where $\boldsymbol{\xi} \in \mathbb{R}^2$, $\hat{\mathbf{x}} \in \mathbb{R}^2$, $\mathbf{u} \in \mathbb{R}^2$, and $y \in \mathbb{R}$.

Define the Lyapunov function $V_p(\boldsymbol{\xi}) = \boldsymbol{\xi}^\top \mathbf{P}\boldsymbol{\xi}$ for all $p \in \mathcal{G}$, with $\mathbf{P}$ as in (23). Considering the dynamics (30), along with (22) and (24), a straightforward calculation yields:

$$\dot{V}_1(\boldsymbol{\xi}) \leq -qV_1, \quad \dot{V}_2(\boldsymbol{\xi}) \leq 0, \quad \dot{V}_3(\boldsymbol{\xi}) \leq -qV_3. \tag{31}$$

Since the function V_p remains the same for all $p \in \mathcal{G}$, for all $\boldsymbol{\xi} \in \mathbb{R}^2$, we have:

$$V_{\sigma(t_i)}(\boldsymbol{\xi}(t_i)) = V_{\sigma(t_{i-1})}(\boldsymbol{\xi}(t_i)), \quad \forall t_i \in \mathfrak{G} \setminus t_0. \tag{32}$$

Therefore, for any $t \in [t_{i-1}, t_i)$ and $p = \sigma(t_{i-1})$, we have:

$$\frac{d}{dt}V_p(\boldsymbol{\xi}) = \dot{V}_p(\boldsymbol{\xi}).$$

Hence, by using (31) and (32), for any $t \in [t_{i-1}, t_i)$, we get:

$$\begin{aligned} V_{\sigma(t_i)}(\boldsymbol{\xi}(t_i)) &= V_{\sigma(t_{i-1})}(\boldsymbol{\xi}(t_i)) \\ &\leq e^{q_p(t_i - t_{i-1})} V_{\sigma(t_{i-1})}(\boldsymbol{\xi}(t_{i-1})), \end{aligned}$$

where we set $q_1 = q_3 = q$ and $q_2 = 0$. Applying this inequality recursively, for any $t \in [t_i, t_{i+1})$, we obtain:

$$V_{\sigma(t_i)}(\boldsymbol{\xi}(t)) \leq c_\sigma(t) V_{\sigma(t_0)}(\boldsymbol{\xi}(t_0)), \tag{33}$$

where:

$$\begin{aligned} c_\sigma(t) &= e^{q_p(t - t_i)} \prod_{k=0}^{i-1} e^{q_p(t_{k+1} - t_k)} \\ &= \prod_{p \in \mathcal{G}} e^{q_p T_p(t_0, t)} \\ &= e^{-q_1 \cdot T_1(t_0, t) - q_3 \cdot T_3(t_0, t)} \\ &\leq e^{-q(T_1(t_0, t) + T_3(t_0, t))} \leq e^{-qc(t - t_0)}. \end{aligned}$$

Here, we used condition (29) in the final step.

Additionally, since the Lyapunov functions satisfy, for all $p \in \mathcal{G}$:

$$\lambda_{\min}(\mathbf{P})\|\boldsymbol{\xi}\|^2 \leq V_p(\boldsymbol{\xi}) \leq \lambda_{\max}(\mathbf{P})\|\boldsymbol{\xi}\|^2, \tag{34}$$

where $\lambda_{\min}(\cdot)$ and $\lambda_{\max}(\cdot)$ are the minimum and maximum eigenvalue of the matrix, respectively, we conclude that for all $t \in [t_i, t_{i+1})$:

$$\begin{aligned} \|\boldsymbol{\xi}(t)\| &\leq \frac{1}{\sqrt{\lambda_{\min}(\mathbf{P})}} V_{\sigma(t_i)}^{\frac{1}{2}}(\boldsymbol{\xi}(t)) \\ &\leq \sqrt{\frac{c}{\lambda_{\min}(\mathbf{P})}} e^{-\frac{q}{2}(t - t_0)} V_{\sigma(t_0)}^{\frac{1}{2}}(\boldsymbol{\xi}(t_0)) \\ &\leq \sqrt{c\frac{\lambda_{\max}(\mathbf{P})}{\lambda_{\min}(\mathbf{P})}} e^{-\frac{q}{2}(t - t_0)} \|\boldsymbol{\xi}(t_0)\|, \end{aligned} \tag{35}$$

which shows that (30) is uniformly globally exponentially stable if (29) holds.

By [15, Proposition 3.1], since (30) is uniformly globally exponentially stable, observer (26) is uniformly contracting according to Definition 3. That is, for any input $\mathbf{u} \in \mathcal{U}$ and any two observer trajectories $\hat{\mathbf{x}}(t)$ and $\hat{\mathbf{x}}'(t)$ in $\mathbf{X}$, there exist constants $a, b > 0$ such that:

$$\|\hat{\mathbf{x}}(t) - \hat{\mathbf{x}}'(t)\| \leq ae^{-bt}\|\hat{\mathbf{x}}(t_0) - \hat{\mathbf{x}}'(t_0)\|. \tag{36}$$

Since the switching signal σ is the same for both the plant (26) and observer (26), $\hat{\mathbf{x}}(t) = \mathbf{x}(t)$ for all $t \geq t_0$ is a solution of observer (26). Thus, (36) implies (12), completing the proof. ■

B. On synchronizing the switching between the observer and the plant

It is important to note that observer (26) must be synchronized with the system mode σ. Thus, developing a method to determine the system's mode is a fundamental aspect of our proposal.

We highlight that, based on (3), the system's mode can be identified by the sign of the normalized sorption mass flow rate f_r. Consequently, if the function f_r can be estimated, the estimation — denoted as $\hat{f}_r$ — can serve as a switching signal to adjust the observer modes. In other words, we propose the following switching mechanism for the observer:

$$\dot{\hat{\mathbf{x}}} = \begin{cases} \mathbf{f_1}\left(\hat{\mathbf{x}}, \mathbf{u}\right) + \frac{\mu}{2}\mathbf{P}^{-1}\mathbf{C}^\top\left(y - \mathbf{C}\hat{\mathbf{x}}\right), & \hat{f}_r > \epsilon_{tol}, \\ \mathbf{f_2}\left(\hat{\mathbf{x}}, \mathbf{u}\right) + \frac{\mu}{2}\mathbf{P}^{-1}\mathbf{C}^\top\left(y - \mathbf{C}\hat{\mathbf{x}}\right), & \left|\hat{f}_r\right| \leq \epsilon_{tol}, \\ \mathbf{f_3}\left(\hat{\mathbf{x}}, \mathbf{u}\right) + \frac{\mu}{2}\mathbf{P}^{-1}\mathbf{C}^\top\left(y - \mathbf{C}\hat{\mathbf{x}}\right), & \hat{f}_r < -\epsilon_{tol}, \end{cases} \tag{37}$$

where ϵ_{tol} is a positive threshold included to account for potential errors during the estimation of f_r.

Next, we need to develop an estimator for the normalized sorption mass flow rate f_r. In this work, we propose using the Unknown System Dynamics Estimator (USDE) introduced in [9]. Specifically, consider the subsystem of (1):

$$\dot{y} = \frac{u_2 - f_r}{v_g}, \tag{38}$$

where y is the density of hydrogen, computed as in (18). We assume that the normalized sorption mass flow rate f_r and its derivative are bounded, i.e.,

$$\sup_{t\geq 0} |\dot{f}_r(t)| \leq \lambda_{fr}$$

for a positive constant $\lambda_{fr} > 0$. This assumption is entirely reasonable in MH tank systems, as all system states and inputs are bounded, and f_r is a piecewise smooth function. Additionally, consider the following low-pass filter for the known variable y and the measured input u_2:

$$\begin{cases} \kappa\dot{u}_{2f} + u_{2f} = u_2, & u_{2f}(0) = 0 \\ \kappa\dot{y}_f + y_f = y, & y_f(0) = 0 \end{cases} \tag{39}$$

where κ is a tunable parameter of the low-pass filter that balances robustness and convergence speed, and u_{2f} and y_f are the filtered versions of u_2 and y, respectively. Based on this, we can define an estimator for the normalized sorption mass flow rate f_r as follows:

$$\hat{f}_r = u_{2f} - v_g \cdot \frac{y - y_f}{\kappa}. \tag{40}$$

The convergence of this estimator is formalized in the following theorem.

Theorem 2 ([9]): Consider (38) *and assume that* $\sup_{t\geq 0}|\dot{f}_r(t)| \leq \lambda_{fr}$ *for some constant* $\lambda_{fr} > 0$*. Then, for all* $t \geq 0$*, the estimator* (40) *satisfies*

$$\|f_r(t) - \hat{f}_r(t)\| \leq \sqrt{e^{-\frac{t}{\kappa}}\|f_r(0) - \hat{f}_r(0)\| + \kappa^2\lambda_{fr}^2}.$$

It is worth noting that decreasing κ improves the convergence rate of the estimator. Additionally, we have:

$$\lim_{t\to\infty} \|f_r(t) - \hat{f}_r(t)\| \leq \kappa\lambda_{fr}. \tag{41}$$

This implies that the estimation error decreases in proportion to the reduction in κ. Based on this result, the threshold in (37) should be selected so that $\epsilon_{tol} > \kappa\lambda_{fr}$, and t_0 in Theorem 1 (the time when the observer begins operation) should be large enough to ensure that $e^{-\frac{t}{\kappa}}\|f_r(0) - \hat{f}_r(0)\| \approx 0$.

V. Numerical simulations

In this section, a numerical simulation is conducted to validate the feasibility of the proposed observation scheme. The temperature evolution is derived from the thermodynamic model of MH tanks, as described in [10]. The parameters utilized in this simulation are listed in Table I, along with additional parameters for the thermal model provided in Table II.

Table II: Thermodynamic model and additional parameters.

Symbol	Value	Symbol	Value
ΔH_a	$2.072 \times 10^4\,\mathrm{J/mol}$	t_{amb}	$298.15\,\mathrm{K}$
c_{pg}	$14\,890\,\mathrm{J/(kg \cdot K)}$	c_{ps}	$6255.4\,\mathrm{J/(kg \cdot K)}$
k_{amb}	$0.7485\,\mathrm{J/(s \cdot K)}$	ρ_{si}	$6363.7\,\mathrm{kg/m^3}$
k_p	0.8487	m_{total}	$0.0315\,\mathrm{kg}$

The observer parameters are set to $\mu = 40$ and $q = 10$. The matrix $\mathbf{P}$ is selected as follows:

$$\mathbf{P} = \begin{bmatrix} 2 & 1 \\ 1 & 1 \end{bmatrix}, \tag{42}$$

which fulfills condition (24).

In the simulation, it is assumed that the initial condition of the MH tank is in the absorption phase, with a switch between charging and discharging occurring within the first 80s. The system inputs, including the normalized mass flow rate f_{in} and the tank temperature t_{tank}, are depicted in Fig. 1. The initial temperature is set at $t_{tank}(0) = 298.15\,\mathrm{K}$.

The initial conditions for the system are specified as $x_1(0) = 0.3253\,\mathrm{kg/m^3}$ and $x_2(0) = 6363.7\,\mathrm{kg/m^3}$, while the observer initial conditions are set to $\hat{x}_1(0) = 0.6\,\mathrm{kg/m^3}$ and $\hat{x}_2(0) = 6390\,\mathrm{kg/m^3}$.

The simulation results are illustrated in Fig. 2. As indicated, the estimation of the sorption rate $\hat{f}_r$ and the estimate $\hat{x}_1$

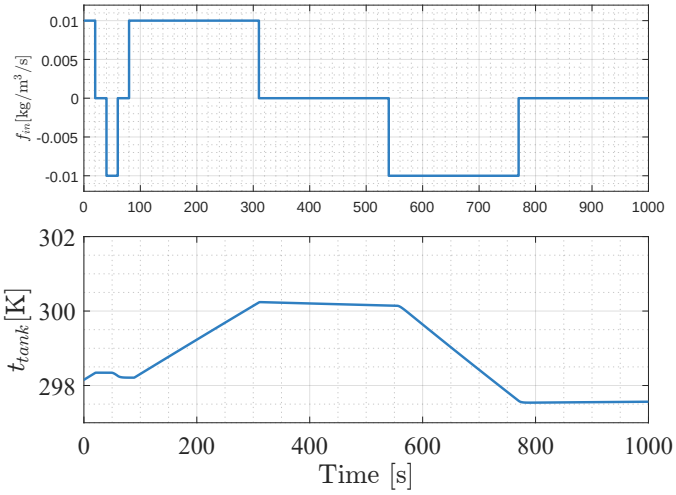

Fig. 1. Evolution of f_{in} and t_{tank} for the system (20) in the simulation.

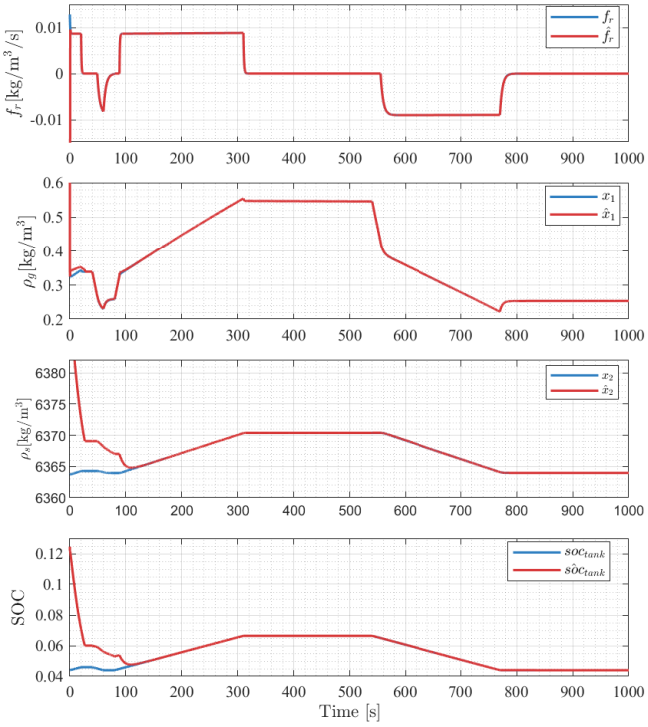

Fig. 2. Comparison of estimator, observer, and SOC estimation results with true values in the simulation.

converge rapidly at the start of the simulation. Moreover, the estimate $\hat{x}_2$ exhibits a stepwise convergence towards x_2, which corresponds to the switching of $\hat{f}_r$ between contractive and non-expansive regions. After around 315s, although the system eventually enters the equilibrium region Ω_2, the observation error remains bounded due to the non-expansive property. Finally, it can be found that the estimation of SOC has the same trend as the estimation of x_2.

VI. Conclusion

This study proposes a nonlinear observer aimed at estimating the density of hydrogen and metal hydride within the MH tank, facilitating further calculations of the tank's SOC. The analysis confirms that the dynamics of the MH tank exhibit differential detectability concerning an Euclidean metric in certain operational regions, while also demonstrating non-expansive behavior in some other. These properties are the foundation for the design of a nonlinear switched observer. Additionally, it has been shown that, under specific switching conditions, the switched observer synchronised with the system, is uniform contraction. The efficacy of the proposed observer and the SOC estimation framework has been verified through a numerical simulation.

References

[1] C. Tarhan and M. A. Çil, "A study on hydrogen, the clean energy of the future: Hydrogen storage methods," *Journal of Energy Storage*, vol. 40, p. 102676, 2021. I

[2] J. Liu, F. Yang, Z. Wu, and Z. Zhang, "A hybrid modeling method of metal hydride tank and dynamic characteristic analysis," *International Journal of Hydrogen Energy*, vol. 50, pp. 799–811, 2024. I

[3] D. Gehring, M. Kölbig, S. Göltz, J. Heidingsfeld, A. Rentz, O. Sawodny, M. Linder, and I. Bürger, "Metal hydride reactor for output temperature control," *International Journal of Hydrogen Energy*, vol. 50, pp. 1502–1517, 2024. I

[4] S. Suarez, D. Chabane, A. N'Diaye, Y. Ait-Amirat, and A. Djerdir, "Static and dynamic characterization of metal hydride tanks for energy management applications," *Renewable Energy*, vol. 191, pp. 59–70, 2022. I

[5] D. Zhu, Y. Ait-Amirat, A. N'Diaye, and A. Djerdir, "On-line state of charge estimation of embedded metal hydride hydrogen storage tank based on state classification," *Journal of Energy Storage*, vol. 42, p. 102950, 2021. I, II-B

[6] X. Wang, H. Su, F. Zhang, and G. Chen, "A robust distributed interval observer design for lti systems," *IEEE Transactions on Automatic Control doi*, vol. 10. I

[7] X. Wang, Z. Fan, L. Wang, H. Su, and J. Lam, "Fully distributed observer design for mobile targets," *IEEE Transactions on Network Science and Engineering*, vol. 10, no. 3, pp. 1696–1708, 2023. I

[8] X. Wang, W. Xu, H. Su, Z. Gao, and G. Chen, "Designing a completely distributed interval observer for the lti system," *IEEE Transactions on Automatic Control*, 2024. I

[9] J. Na, B. Jing, Y. Huang, G. Gao, and C. Zhang, "Unknown system dynamics estimator for motion control of nonlinear robotic systems," *IEEE Transactions on Industrial Electronics*, vol. 67, no. 5, pp. 3850–3859, 2019. 2, IV-B, 2

[10] M. Chen, C. Batlle, B. Escachx, R. Costa-Castelló, and J. Na, "Sensitivity analysis and calibration for a two-dimensional state-space model of metal hydride storage tanks based on experimental data," *Journal of Energy Storage*, vol. 94, p. 112316, 2024. II-A, V

[11] P. Bernard, V. Andrieu, and D. Astolfi, "Observer design for continuous-time dynamical systems," *Annual Reviews in Control*, vol. 53, pp. 224–248, 2022. 1, III-A

[12] A. Duvall and E. D. Sontag, "A remark on omega limit sets for non-expansive dynamics," 2024. [Online]. Available: https://arxiv.org/abs/2404.02352 2

[13] F. Bullo, "Contraction theory for dynamical systems," *Kindle Direct Publishing*, 2024. 3

[14] S. Boyd, L. El Ghaoui, E. Feron, and V. Balakrishnan, *Linear matrix inequalities in system and control theory*. SIAM, 1994. III-B

[15] H. Yin, B. Jayawardhana, and S. Trenn, "On contraction analysis of switched systems with mixed contracting-noncontracting modes via mode-dependent average dwell time," *IEEE Transactions on Automatic Control*, vol. 68, no. 10, pp. 6409–6416, 2023. IV-A, IV-A